JOURNAL OF AIRCRAFT
Vol. 48, No. 2, March–April 2011

Engineering Notes

Limit Cycle Oscillations of Plate-Type Fins Using Increased-Order Models

Dani Levin* and Moti Karpel†
Technion-Israel Institute of Technology, Haifa 32000, Israel

DOI: 10.2514/1.C031102

I. Introduction

AEROELASTIC considerations in the structural design of flight vehicles, such as flutter boundaries and dynamic gust loads, are usually based on linear structural and aerodynamic models. Being required by certification regulations to be used in an adequately accurate or conservative manner, the use of such tools might yield overdesigned vehicles with inferior performance, and/or require costly verification tests. The account for nonlinear effects may lead in such cases to improved and/or cheaper products.

Extensive research has been conducted in recent years on reduced-order modeling of aeroelastic systems that starts with high-fidelity nonlinear computational schemes. The alternative increased-order modeling (IOM) approach used in this work attempts to model nonlinear aeroelastic systems in a different way. It is based on linear models that are supplemented with nonlinear feedback loops that simulate local nonlinearities identified from high-fidelity models or tests. Generally, the addition of nonlinear elements to linear models has been in use by engineers for many years, one way or another, when dealing with nonlinear systems. Recent IOM projects [1,2] aimed at the development of a systematic framework that exploits as much as possible the numerical advantages in dealing with linear systems while keeping the complexity of the added nonlinear elements as low as required for obtaining adequate accuracy in aeroelastic applications.

The emerging IOM framework is based on the two schemes of [2] for dynamic loads of linear aeroelastic system with a control system that includes significant nonlinear elements such as displacement limits and activation zones. A typical IOM block diagram in this case is shown in Fig. 1. The solution sequence starts in the first scheme with the calculation of frequency response functions of the linear aeroelastic system. The modal response is then calculated using fast-Fourier-transform (FFT) techniques [3,4] with the nonlinear elements replaced by linear ones. The response is then corrected by incremental nonlinear effects in a process that combines time domain solutions of the nonlinear elements and convolution integrals for the linear parts with impulse response functions based on the frequency-domain plant model. The second scheme is based on time domain models that use rational-function approximation of the unsteady aerodynamic force coefficients to generate state-space aeroservoelastic equations of motion [5] that can accommodate nonlinear control elements in using common utility software packages such as Matlab/Simulink.

The research described in this paper applied the IOM approach to the simulation of limit-cycle oscillations (LCO) of plate-type fins with nonlinearity due to stress stiffening of the middle plane of the plate elements in bending. The main purposes were the advancement of the IOM technology, the development of practical tools for solid fin design with LCO considerations, and the identification of the main driver of aeroelastic LCO of such fins. The test case is the cropped delta wing that was tested at the NASA Ames Research Center wind tunnel [6] and showed several LCO incidences. The case was analyzed using direct time marching processes with fully nonlinear models [7–9]. The dimensions and the structural model of the 0.9 mm-thick cropped delta wing are shown in Fig. 2.

II. Structural Model

The basic equation of motion of the structure in discrete coordinates is

$$[m]\{\ddot{u}\} + [c]\{\dot{u}\} + [k]\{u\} = \{F_A(t)\} \tag{1}$$

where m, k, and c are the mass, stiffness, and damping matrices, respectively, $\{u\}$ is the structural displacement vector, and $\{F_A(t)\}$ is the vector of unsteady aerodynamic forces. Our work focuses on the structural nonlinearity arising from stress stiffening of platelike fins in bending. To represent this stiffness addition, the nonlinear von Kármán plate strain equations are used [10,11]

$$\varepsilon = \begin{Bmatrix} \varepsilon_L^{\mathrm{pl}} + \varepsilon_{NL}^{\mathrm{pl}} \\ \varepsilon_L^{b} \end{Bmatrix} \tag{2}$$

where $\{\varepsilon_L^{\mathrm{pl}}\}$, $\{\varepsilon_L^{b}\}$ and are the linear in-plane and bending strain vectors, respectively, and $\{\varepsilon_{NL}^{\mathrm{pl}}\}$ is the nonlinear strain vector added due to midplane stretching while the plate bends

$$\left\{\varepsilon_L^{\mathrm{pl}}\right\} = \begin{Bmatrix} \frac{\partial u}{\partial x} \\ \frac{\partial v}{\partial y} \\ \frac{\partial u}{\partial y} + \frac{\partial v}{\partial x} \end{Bmatrix}; \qquad \left\{\varepsilon_L^{b}\right\} = \begin{Bmatrix} -\frac{\partial^2 w}{\partial x^2} \\ -\frac{\partial^2 w}{\partial y^2} \\ 2\frac{\partial^2 w}{\partial x \partial y} \end{Bmatrix};$$
$$\left\{\varepsilon_{NL}^{\mathrm{pl}}\right\} = \begin{Bmatrix} \frac{1}{2}\left(-\frac{\partial w}{\partial x}\right)^2 \\ \frac{1}{2}\left(\frac{\partial w}{\partial y}\right)^2 \\ \left(\frac{\partial w}{\partial x}\right)\left(\frac{\partial w}{\partial y}\right) \end{Bmatrix} \tag{3}$$

Platelike fins are usually modeled with 4-node plate elements. An element has 5 degrees of freedom at each node: u and v translations in the x and y in-plane directions, w in the z out-of-plane direction, and θ_x, θ_y rotations about x and y. Polynomial shape functions are used to represent strain terms as a function of the nodal displacements and rotations. Different shape functions were used for in-plane and bending strain terms:

$$u(x,y) = [\overline{XY}_{\mathrm{plane}}][XY_{\mathrm{plane}}]^{-1}\{u^e\}$$
$$v(x,y) = [\overline{XY}_{\mathrm{plane}}][XY_{\mathrm{plane}}]^{-1}\{v^e\} \qquad w(x,y) = [\overline{XY}][XY]^{-1}\{\delta_b^e\} \tag{4}$$

where the $[\overline{XY}_{\mathrm{plane}}]$ and $[\overline{XY}]$ matrices include polynomial coefficients, while $[XY_{\mathrm{plane}}]^{-1}$ and $[XY]^{-1}$ are matrices of constants. The $\{u^e\}$ and $\{v^e\}$ vectors consist of nodal in-plane translations in the x and y direction, respectively, for each node in the element, four

Presented as Paper 2010-2634 at the 51st AIAA/ASME/ASCE/AHS/ASC Structures, Structural Dynamics and Materials Conference, Orlando, FL, 12–15 April 2010; received 10 May 2010; revision received 2 December 2010; accepted for publication 2 December 2010.

*Graduate Student, Faculty of Aerospace Engineering.
†Professor, Faculty of Aerospace Engineering, Sanford Kaplan Chair for Aerospace Engineering. Associate Fellow AIAA.

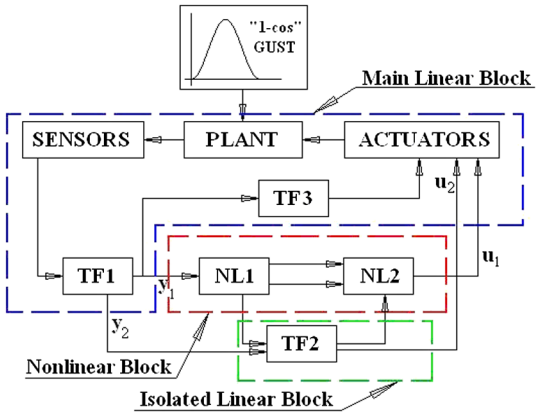

Fig. 1 Blocks of IOM for gust response with nonlinear control.

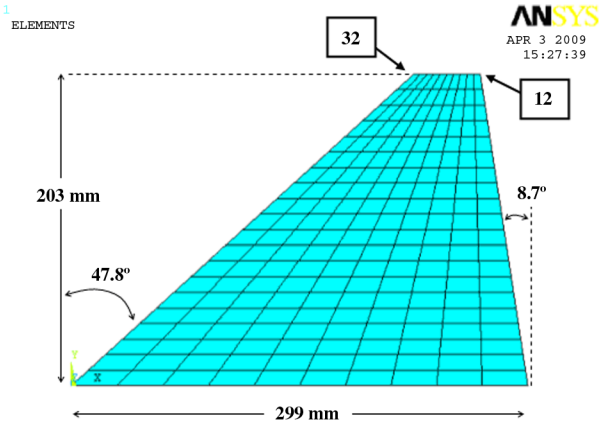

Fig. 2 Structural model of the cropped delta wing.

terms in each vector. $\{\delta_b^e\}$ consists of the out-of-plane deflection w and the two rotations θ_x, θ_y for each node in the element, 12 terms in the vector. Rotations can be extracted easily by differentiating the third shape function:

$$\theta_x = -\frac{\partial w}{\partial y}: \theta_y = \frac{\partial w}{\partial x} \tag{5}$$

Linear finite element matrices can be extracted by substituting Eqs. (4) and (5) into the linear parts of Eq. (2). Simple expressions are obtained for the in-plane and bending linear strain matrices [11]:

$$\{\varepsilon_L^{\text{pl}}\} = [B_L^{\text{pl}}]\{\delta_{\text{pl}}^e\}; \qquad \{\varepsilon_L^b\} = [B_L^b]\{\delta_b^e\} \tag{6}$$

where $\{\delta_{\text{pl}}^e\}$ consists of the in-plane displacements $\{v^e\}$ and $\{u^e\}$. The nonlinear part of the strain vector is expressed as

$$\{\varepsilon_{NL}^{\text{pl}}\} = [B_{NL}^{\text{pl}}]\{\delta_b^e\} \tag{7}$$

where

$$[B_{NL}^{\text{pl}}] = \frac{1}{2}\begin{bmatrix} \frac{\partial \overline{XY}}{\partial x} & 0 \\ 0 & \frac{\partial \overline{XY}}{\partial y} \\ \frac{\partial \overline{XY}}{\partial y} & \frac{\partial \overline{XY}}{\partial x} \end{bmatrix}\begin{bmatrix} [XY]^{-1} & 0 \\ 0 & [XY]^{-1} \end{bmatrix}\begin{bmatrix} \{\delta_b^e\} & 0 \\ 0 & \{\delta_b^e\} \end{bmatrix}\begin{Bmatrix} \frac{\partial \overline{XY}}{\partial x} \\ \frac{\partial \overline{XY}}{\partial y} \end{Bmatrix}[XY]^{-1}$$

The total stiffness matrices of a plate element is calculated by

$$[K^e] = [K_L^e] + [K_{NL}^e] = \int_V [B]^T[D][B]\,\mathrm{d}v \tag{8}$$

where

$$[B] = \begin{bmatrix} B_L^{\text{pl}} & B_{NL}^{\text{pl}} \\ 0 & B_L^b \end{bmatrix}; \qquad [D] = \begin{bmatrix} D^{\text{pl}} & 0 \\ 0 & D^b \end{bmatrix}$$

where

$$D^{\text{pl}} = \frac{Eh}{1-\nu^2}\begin{bmatrix} 1 & \nu & 0 \\ \nu & 1 & 0 \\ 0 & 0 & (1-\nu^2)/2 \end{bmatrix};$$

$$D^b = \frac{Eh^3}{12(1-\nu^2)}\begin{bmatrix} 1 & \nu & 0 \\ \nu & 1 & 0 \\ 0 & 0 & (1-\nu^2)/2 \end{bmatrix}$$

where E is the Young's elastic modulus, ν is the Poisson's ratio, and h is the thickness of the plate. The resulting linear and nonlinear parts of the element stiffness matrix are

$$[K_L^e] = \int_V \begin{bmatrix} B_L^{\text{pl}T} D^{\text{pl}} B_L^{\text{pl}} & 0 \\ 0 & B_L^{bT} D^b B_L^b \end{bmatrix}\mathrm{d}v \tag{9}$$

and

$$[K_{NL}^e] = \int_V \begin{bmatrix} 0 & B_0^{\text{pl}T} D^{\text{pl}} B_{NL}^{\text{pl}} \\ B_{NL}^{\text{pl}T} D^{\text{pl}} B_0^{\text{pl}} & B_{NL}^{\text{pl}T} D^{\text{pl}} B_{NL}^{\text{pl}} \end{bmatrix}\mathrm{d}v \tag{10}$$

Note the difference between the linear and nonlinear expressions for the stiffness matrices. The linear stiffness matrix (9) is constant and depends only on the geometry of the element, thus has to be calculated only once. The nonlinear expression (10) depends on the structural deformations through $\{\delta_b^e\}$ in $[B_{NL}^{\text{pl}}]$ of Eq. (7), hence needs to be repeatedly updated during calculations.

Plate structures often experience large levels of deformation while the strain levels remain small. When the stiffness matrices are calculated with the total deformation vectors, excessive nonlinear stiffness might be obtained. The element-independent corotational (CR) approach [12] of treating large deflections and rotations is used to avoid excessive stiffening. In this approach, the total deformation vector is decomposed into rigid body motion and elastic deformations as illustrated in Fig. 3

$$\{\delta_b^e\} = \{\delta_b^e\}_{\text{Rigid}} + \{\delta_b^e\}_{\text{elastic}} \tag{11}$$

and the nonlinear stiffness matrix is calculated by Eq. (10) using the deformational part only, $\{\delta_b^e\}_{\text{elastic}}$. A convenient way for calculating the deformational part [13] is by attaching a reference plane to the deformed element, and then calculating $\{\delta^e\}_{\text{elastic}}$ relative to this plane.

The global stiffness matrix of Eq. (1) is constructed in two parts, the linear k_L in which all the element K_L^e matrices are assembled, and the nonlinear $k_{NL}(u)$ in which all the element K_{NL}^e matrices are assembled. For computational efficiency and for compatibility with standard aeroelastic modeling, Eq. (1) is transformed to generalized coordinates by assuming

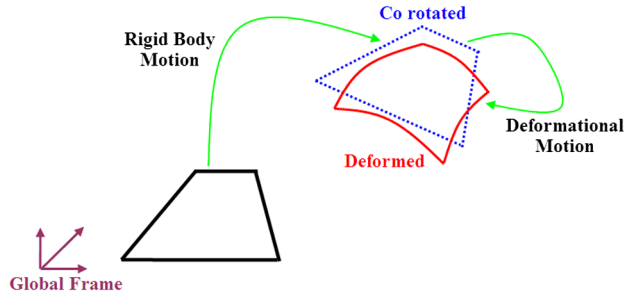

Fig. 3 Corotational decomposition into rigid-body and elastic displacements.

$$\{u\} = [\phi]\{\xi\} \tag{12}$$

where ϕ is the matrix of low-frequency natural vibration modes calculated with a linear finite element model whose stiffness matrix is k_L, and ξ is the vector of generalized displacement, defining the contribution of each mode to the total deformations. The substitution of Eq. (12) in Eq. (1) and the premultiplication by $[\phi]^T$ yield

$$[M]\{\ddot{\xi}\} + [C]\{\dot{\xi}\} + ([K_L] + [\Delta K(\xi)])\{\xi\} = [\phi]^T\{F_A(t)\} \tag{13}$$

where M and K_L are diagonal due to the modal orthogonality, C is also commonly assumed to be diagonal, and

$$[\Delta K(\xi)] = [\phi]^T[k_{NL}(u)][\phi] \tag{14}$$

The generalized aerodynamic forces are discussed in the next section.

III. Aeroelastic Model

The aerodynamic model is based on commonly used frequency-domain unsteady panel models such as those of MSC/NASTRAN or ZAERO. Several complex generalized force coefficient matrices $Q(ik)$ that are associated with are calculated at selected $k = \omega L/V$ reduced frequency values, where ω is the frequency of oscillations, L is a reference length, and V is the air velocity. Rational function approximation of $[Q(ik)]$ using the minimum-state formulation [5] in ZAERO, based on the tabulated $Q(ik)$, yields the real coefficient matrices in

$$[\tilde{Q}(ik)] = [A_0] + \frac{L}{V}[A_1]ik + \frac{L^2}{V^2}[A_2](ik)^2 + [D]\left([I]ik - \frac{V}{L}[R]\right)^{-1}[E]ik \tag{15}$$

The replacement of ik in Eq. (15) by the Laplace variable s, the addition of an aerodynamic augmenting vector $\{x_a\}$ that represents the lags in the development of the unsteady aerodynamic forces, the replacement of the right-hand side of Eq. (13) by $q[\tilde{Q}(s)]\{\xi(s)\}$ and the transformation of this term to the time domain, yield the state-space equations

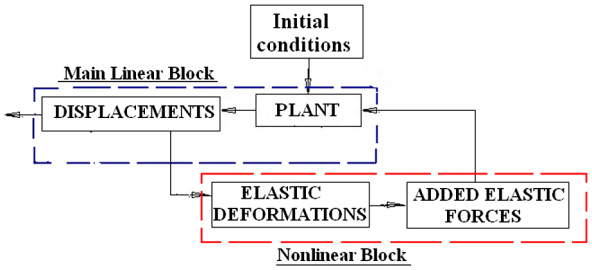

Fig. 4 Block diagram of IOM for aeroelastic response of platelike fin.

$$\begin{Bmatrix} \dot{\xi} \\ \ddot{\xi} \\ \dot{x}_a \end{Bmatrix} = \begin{bmatrix} 0 & I & 0 \\ [\bar{M}]^{-1}[K + qA_0] & -[\bar{M}]^{-1}\left[C + \frac{qL}{V}A_1\right] & -q[\bar{M}]^{-1}[D] \\ 0 & [E] & \frac{V}{L}[R] \end{bmatrix} \times \begin{Bmatrix} \xi \\ \dot{\xi} \\ x_a \end{Bmatrix} - \begin{Bmatrix} 0 \\ [\bar{M}]^{-1}[\Delta K(\xi)] \\ 0 \end{Bmatrix}\{\xi\} \tag{16}$$

where $[\bar{M}] = [M] + \frac{qL^2}{V^2}[A_2]$.

IV. Increased-Order Modeling Process

The IOM block diagram that reflects Eq. (16) with the nonlinear feedback based on $\Delta K(\xi)$ which results from Eqs. (11–14) is shown in Fig. 4. The PLANT box contains the linear part of Eq. (16). The DISPLACEMENTS box converts the modal response $\{\xi(t)\}$ into discrete displacements at the finite element degrees of freedom. The corotational approach is used in the nonlinear block to separate the rigid-body and elastic deformations of each element and the elastic deformations are used for calculating the added nonlinear elastic forces. The nonlinear addition in static computations is calculated iteratively, typically converging in 3–4 iterations. In dynamic simulations with small-enough time steps, the iterative process may be avoided. The added nonlinear forces are converted to generalized coordinates and expressed as ΔK in the ADDED ELASTIC FORCES block. The resulting added generalized forces are fed back to Eq. (16) in a time-marching process.

To summarize the IOM process, we recall the modeling steps. The first step includes linear finite element modeling and modal analysis for extracting the natural frequencies and normal modes. A linear flutter analysis is performed in the second step. The dynamic properties of the structure are taken from the modal analysis. Aerodynamic matrices are constructed for a given Mach number and air density. The rational approximation of Eq. (15) leads to the state-space Eq. (16) without the right-hand feedback term. The linear flutter analysis is performed by extracting the eigenvalues of the system matrix for increasing air velocities. The flutter velocity is the velocity at which the real part of an eigenvalue branch becomes positive. At the third step a linear aeroelastic system is constructed for velocities above flutter speed and a time-marching response from arbitrary initial conditions is performed, using standard utility routines, to verify that the response diverges at about the flutter frequency. At the fourth step the nonlinear block is added, thus closing the nonlinear loop, and LCO investigation is performed.

V. Numerical Example

The cropped delta wing model of Fig. 2 was used for the LCO investigation. The wing is made of a steel plate with a constant thickness of 0.9 mm and the following elastic properties: $E = 2.10^{11}$ Pa $\nu = 0.25$; $\rho_{St} = 7850$ kg/m^3. Modal analysis was performed using the ANSYS code with linear plate elements. Natural frequencies and mode shapes are evaluated by finding the eigenvalues and eigenvectors of Eq. (1) without the damping matrix and with no external forces. The first three evaluated natural frequencies are 26.7, 88.8, and 132.9 Hz. The corresponding mode shapes are shown in Fig. 5. These are the first-bending,

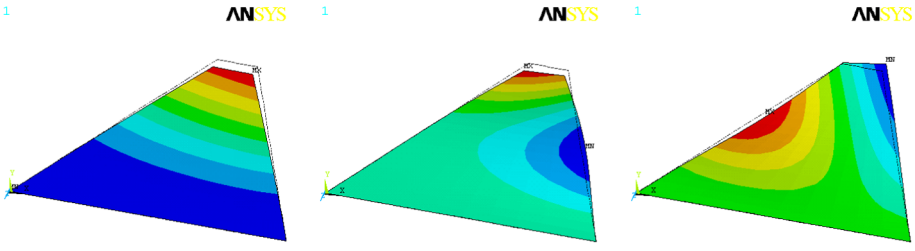

Fig. 5 Three lowest-frequency elastic modes.

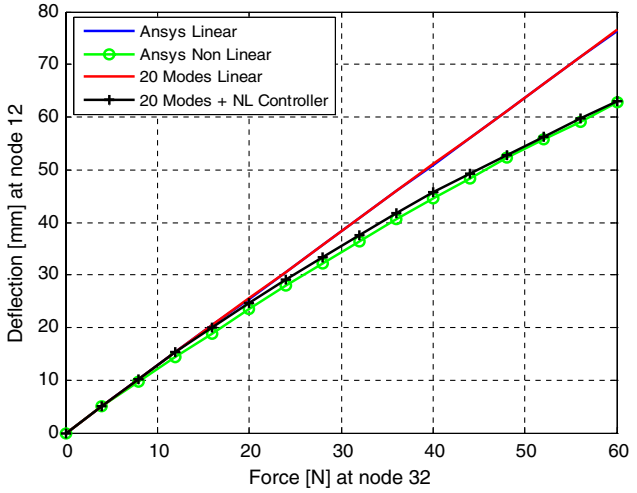

Fig. 6 Linear and nonlinear static displacement curves.

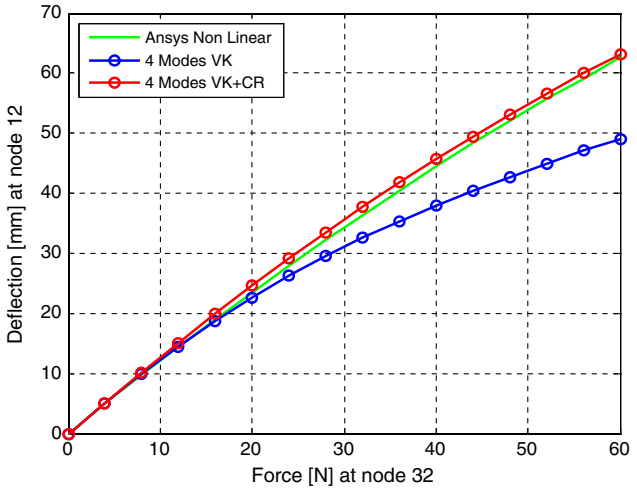

Fig. 7 Nonlinear static displacement curves with and without corotational correction.

second-bending, and first torsion modes, which are the most important in following aeroelastic analyses. The inclusion of in-plane modes in the linear part of the model is less important as they do not interact with the aerodynamic loads. However, the stiffening effects of the in-plane displacements are still considered in the nonlinear stiffness increments.

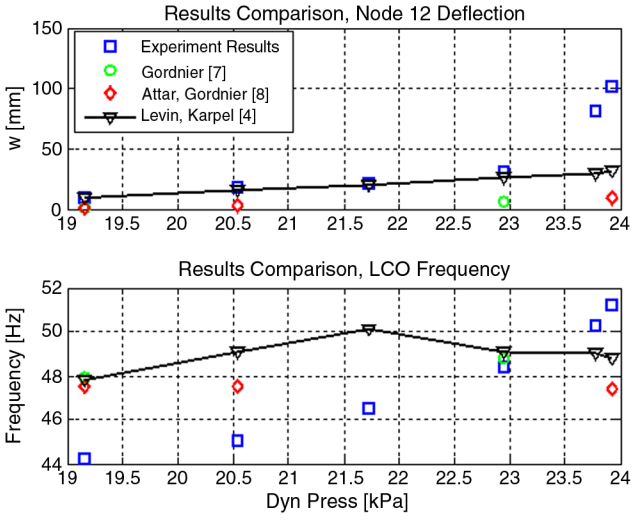

Fig. 8 Comparison between LCO test results and numerical solutions.

The accuracy of the nonlinear feedback forces was first checked by solving the static version of Eq. (13) for the response to a static excitation force at point 32 of Fig. 2 with no aerodynamics

$$([K_L] + [\Delta K(\xi)])\{\xi\} = \{F_{\text{ext}}\} \tag{17}$$

where $\{F_{\text{ext}}\}$ is a vector of generalized forces based on a constant vertical force at point 32 of Fig. 2 and zero elsewhere. An iterative solution of Eq. (17) for $\{\xi\}$, followed by the recovery of the vertical displacement at point 12, yielded the deflection curves of Fig. 6 where the 20-mode nonlinear-controller solution and the respective linear solution are compared with a full direct-coordinate solutions by ANSYS. It can be observed that the linear solutions are practically identical and that the differences between the nonlinear solutions are small. Modal convergence studies showed that good accuracy is obtained with only four modes. Hence only four lowest-frequency modes were used for extracting the following results.

The influence of the number of elastic modes that are taken into account was checked by repeating the static analysis with 4, 10, and 20 first elastic modes. The comparison shows that there is a small difference between the results when the number of modes increases, but still the solution is closer to that of ANSYS when the number of modes is increased. For the following results, only four lowest-frequency modes were used.

A comparison was also made between two static nonlinear structural models, with and without the corotational corrections. The results are compared in Fig. 7. It is clear that without the use of the corotational correction the model is way too stiff.

The linear part of the state-space aeroelastic equation of motion (16) was constructed using ZAERO with five aerodynamic lag states. Linear flutter analysis via eigenvalue extraction of the system matrix indicated a torsion-bending flutter mechanism at Mach 0.85, $q_f = 18.96$ kPa, $\omega_f = 45.6$ Hz. Nonlinear simulations at higher dynamic pressures resulted in diverging amplitudes up to a point where constant LCO amplitudes were obtained. The LCO amplitudes and frequencies are compared in Fig. 8 with the experimental results of [6] and with the computational results of [8,9]. Excellent results are shown for the LCO amplitudes of our model up to 23 kPa. The divergence of the experimental amplitudes at high dynamic pressures may be related to the root cracks that were discovered at the end of the wind tunnel tests. The LCO frequencies with our model are up to 8% off the experimental frequencies, similarly to the other numerical results.

VI. Conclusions

The IOM approach was successfully applied to LCO investigation with stress stiffening plate nonlinearity. Being based on common linear aeroelastic models, the resulting process is efficient, robust, and provides a natural extension to existing industrial numerical procedures. With the nonlinear parts defined in a separate feedback block, the IOM approach provides a framework for implementation of various kinds of nonlinearities while keeping the basic linear model and taking advantage of the linearity of the main block. The developed process provides a general numerical tool for LCO investigation with plate-type fin models of any geometry. The application to the cropped delta wing demonstrated the process validity. The excellent agreement with test results shows that the first nonlinear term in von Kármán's nonlinear plate strain equation is indeed the main driver of the LCO process in these cases. The results show that an adequate LCO investigation of unattended flight vehicles, with models similar to those of this work, may allow lower and even negative flutter margins and hence lead to cheaper and/or more efficient designs.

References

[1] Karpel, M., Hollander, Y., Gur, I. E., and Levy, Y., "Increased-Order Models for the Prediction of Aeroelastic Limit Cycle Oscillations," AIAA Paper 2008-1757, April 2008.

[2] Karpel, M., Shousterman, A., Maderuelo, C., Anguita, L., and Climent, H., "Dynamic Gust Response with Nonlinear Control Using Frequency

Domain Models," *Proceedings of the International Forum on Aeroelasticity and Structural Dynamics*, CEAS Paper 2009-107, June 2009.

[3] Karpel, M., Moulin, B., Presente, E., Anguita, L., Maderuelo, C., and Climent, H., "Dynamic Response To Gust Excitation With Nonlinear Control Systems," *Proceedings of the International Forum on Aeroelasticity and Structural Dynamics*, CEAS Paper 2007-IF-072, Stockholm, Sweden, June 2007.

[4] Karpel, M., Feldgun, V., and Moulin, B., "Dynamic Response of Aeroelastic Systems Using Fast Fourier Transforms," *Proceedings of the International Forum on Aeroelasticity and Structural Dynamics*, CEAS Paper 2007-IF-049, Stockholm, Sweden, June 2007.

[5] Karpel, M., "Time-Domain Aeroservoelastic Modeling Using Weighted Unsteady Aerodynamic Forces," *Journal of Guidance, Control, and Dynamics*, Vol. 13, No. 1, 1990, pp. 30–37. doi:10.2514/3.20514

[6] Schairer, E. T., and Hand, L. A., "Measurements of Unsteady Aeroelastic Model Deformation by Stereo Photogrammetry," NASA Ames Research Center, 94035, Moffett Field, CA, 1997.

[7] Attar, P. J., Dowell, E. H., and White, J. R., "Modeling Delta Wing Limit-Cycle Oscillations Using a High-Fidelity Structural Model," *Journal of Aircraft*, Vol. 42, No. 5, Sept.–Oct. 2005, pp. 1209–1217. doi:10.2514/1.11325

[8] Gordnier, R. E., "Computation of Limit-Cycle Oscillations of a Delta Wing," *Journal of Aircraft*, Vol. 40, No. 6, 2003, pp. 1206–1208. doi:10.2514/2.7212

[9] Attar, P. J., and Gordnier, R. E., "Aeroelastic Prediction of the Limit Cycle Oscillations of a Cropped Delta Wing," *Journal of Fluids and Structures*, Vol. 22, No. 1, 2006, pp. 45–58. doi:10.1016/j.jfluidstructs.2005.08.010

[10] Novozhilov, V. V., *Foundations of the Nonlinear Theory of Elasticity*, Dover, New York, 1999.

[11] Dowell, E. H., "Aeroelasticity of Plates and Shells," Noordhoff International Publishing, Leyden, The Netherlands, 1975.

[12] Rankin, C. C., and Brogan, F. A., "An Element Independent Corotational Procedure for the Treatment of Large Rotations," *Journal of Pressure Vessel Technology*, Vol. 108, No. 2, May 1986, pp. 165–174. doi:10.1115/1.3264765

[13] Rankin, C. C., "Application of Linear Finite Elements to Finite Strain Using Corotation," *AIAA/ASME/ ASCE/AHS/ASC Structures, Structural Dynamics, and Material Conference*, AIAA Paper 2006-1751, 2006.